# Numerical modeling of an integrating sphere radiation source

Alexander V. Prokhorov and Leonard M. Hanssen*

National Institute of Standards and Technology, 100 Bureau Dr., Gaithersburg,
MD 20899-8441, USA

## ABSTRACT

Integrating spheres are often used as calibration sources providing uniform radiance within a solid angle and/or uniform irradiance at a distance. The best performance in such a system can be achieved if one is able to evaluate as well as predict the important characteristics of the sphere system's output, such as the spatial and angular distributions of radiance over the exit port, or the distribution of irradiance at the external plane of calibration. We have developed the algorithms and specialized software based on Monte Carlo techniques to solve the problem of radiation transfer inside an integrating sphere containing several point sources and conical annular baffle. The new algorithm employs backward ray tracing coupled with the "shadow rays" technique. As a timesaving procedure, the axial symmetry of the sphere and the superposition principle are used to substitute the sum of single source radiation fields rotated through a specific angle, for the radiation field of the complete multiple source sphere. The random (due to the stochastic character of the Monte Carlo method) component of uncertainty for the radiance or irradiance results is less than 0.1%. The results of numerical experiments are used to establish the performance variation as a function of the reflectance and specularity of the sphere wall, the number of radiation sources, the type of baffle used, and the angular distribution of their radiant intensity.

**Keywords:** integrating sphere, uniform source, radiance, irradiance, calibration, Monte Carlo, simulation, modeling, ray tracing

## 1. INTRODUCTION

Integrating spheres are technically unsophisticated devices that are nevertheless very widely used in photometry, radiometry and related fields. Among numerous applications, integrating spheres are often used as extended-area calibration sources of uniform radiance, or as a source providing uniform irradiance at a distance [1, 2]. In order to achieve the best performance for an integrating sphere radiation source (ISRS), one should be able to evaluate and predict the most important characteristics of the sphere source's output, such as the spatial and angular distributions of radiance over the exit port, or the distribution of irradiance at the external plane of calibration.

Although the theory of an ideal integrating sphere is very simple, deviations from Lambert's law for reflections off its internal surfaces, as well as the presence of ports and baffles make a non-trivial problem of the exact computation of its characteristics. A number of analytical and numerical methods [3-6] have been developed to resolve this problem. The common disadvantages of these methods are well known: their applicability to only Lambertian surfaces and the growth of computational difficulties with the sophistication of system geometry. In the last decades, very important results in computer modeling of integrating sphere have been obtained with the help of the Monte Carlo method [7-13]

The foundation of this technique is the probabilistic treatment of radiation-matter interactions. This approach allows construction of a stochastic model of the system being modeled and an assessment of its parameters with a large number of ray tracing implementations. The number of realizations of a stochastic process determines the accuracy of the solutions.

## 2.  OBJECTIVES

In this paper we demonstrate the usefulness of the computational method through the example of computer modeling of the ISRS, which is intended to calibrate detectors in both spectral radiance and irradiance modes. The primary requirement for these calibrations is the uniformity of the radiance distribution over a solid angle subtended by the exit port of integrating sphere, and/or high uniformity of the irradiance distribution on a plane, for instance, where detector arrays could be calibrated.

The objectives of this work are the following:
- Develop an algorithm and computer code intended for the calculation of (1) the radiance produced by the ISRS at any given point and in any given direction as well as (2) the irradiance at any given point of a plane;
- Perform preliminary parametric studies of radiance and irradiance distributions produced by the ISRS.

## 3.  COMPUTATIONAL MODEL

Because we consider only monochromatic sources, we shall omit the modifier "spectral" in the terms and lower indices "$\lambda$" for radiometric quantities and in equations.

We assume geometrical (ray) optics and do not consider diffraction effects. We also assume that either the radiation source emits unpolarized radiation, or that light is effectively depolarized by multiple reflections.

### 3.1  Geometry
A schematic cross section of the ISRS and embedded coordinate system are depicted in Figure 1. The model of the ISRS includes the sphere's internal surface 1; an annular baffle with sides 2 and 3, which is part of a conical surface whose vertex coincides with the origin of the coordinate system, and the coordinate axis $z$ on which is centered the flat diaphragm 4 with aperture 0, as well as the plane 6 for irradiance measurements; the radiation point source is located at 5.
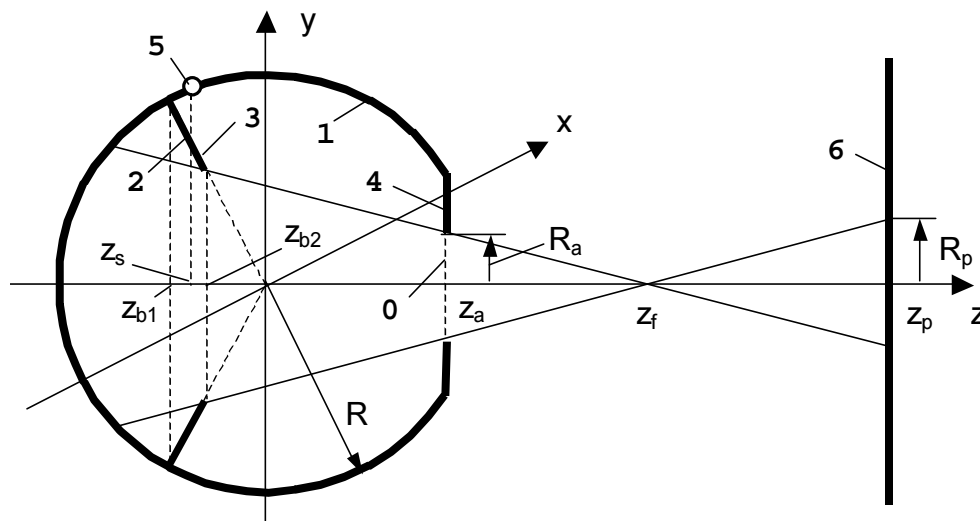


Figure 1: Integrating sphere radiation source. 0. Exit port. 1. Internal spherical surface.
2 and 3. Two sides of conical baffle. 4. Flat diaphragm. 5. Point source. 6. Normal plane

For calibration in radiance mode, the choice of point $z_f$ for observation ensures that the field of view is limited by the aperture diaphragm and the edges of the conical baffle.

## 3.2 Reflectance

The uniform specular-diffuse model of reflection has been used for components of the ISRS. According to this model, the directional-hemispherical reflectance is a sum of perfectly diffuse (Lambertian) and specular components, and both components do not depend on incident angle. Each surface can be characterized by the value of specularity:

$$S = \rho_s / (\rho_s + \rho_d) = \rho_s / \rho,$$

where $\rho_s$ and $\rho_d$ are the specular and diffuse components of reflectance, respectively, and $\rho$ is their sum.

The type of reflection – relative diffuse and specular components – is chosen randomly by means of the specularity $S$. If a pseudo-random number $\eta_s$ produced by the program's pseudo-random number generator (PRNG) is less than the value of specularity $S$, then the reflection is considered to be specular, otherwise it is diffuse. The direction of the specular reflection can be computed by the equation

$$\vec{\omega}_r = \vec{\omega}_i - 2(\vec{n} \cdot \vec{\omega}_i)\vec{n}$$

where $\vec{\omega}_r$, $\vec{\omega}_i$ and $\vec{n}$ are vectors of the direction of reflection, direction of incidence, and the normal to the surface at the incidence point, respectively.

The conventional method (see, for instance, [14]) to generate random directions for the Lambertian component involves computation of the coordinates $\theta$ and $\phi$ of the local spherical coordinate system after simple transformation of a pair of pseudo-random numbers $\eta_\theta$ and $\eta_\phi$ according to

$$\begin{cases} \theta = \arcsin \sqrt{\eta_\theta}, \\ \phi = 2\pi\eta_\phi \end{cases},$$

with the subsequent transformations first to the local Cartesian coordinate system and then to the global one.

The speed of the search for the ray intercept with the spherical surface after diffuse reflection from the same surface can be significantly increased by using the following fact: the surface of any sphere, which is tangent to the surface of a Lambertian reflector in the point of reflection, is a surface of uniform irradiance. Hence, in order to model the chain of diffuse reflection points on the internal surface of a sphere, it is sufficient to generate the chain of points uniformly distributed over this surface. We used the algorithm of G. Marsaglia [15] to obtain the points uniformly distributed on the spherical surface $x^2 + y^2 + z^2 = 1$. The algorithm consists in the following. After a linear transformation of the pair of pseudo-random numbers $\eta_x$ and $\eta_y$:

$$\begin{cases} u_x = 2\eta_x - 1; \\ u_y = 2\eta_y - 1 \end{cases},$$

where the points with coordinates $x = u_x$ and $y = u_y$ are uniformly distributed within the square $(-1 < x, y < 1)$. If $s = u_x^2 + u_y^2 > 1$ (a point is outside the circle of unit radius), the pair of pseudo-

random numbers $\eta_x$ and $\eta_y$ is rejected, and a new pair is generated. Otherwise, the coordinates of the point on the surface of the unit sphere are

$$\begin{cases} x = 2u_x\sqrt{1-s}; \\ y = 2u_y\sqrt{1-s}; \\ z = 1-2s. \end{cases}$$

For a sphere of radius $R$, the coordinates of the point in previous equation must be multiplied by $R$.


### 3.3 Radiation sources

In practice, the several types of radiation sources may be employed: laser beam coupled with diffuser; laser radiation input through the special small opening in spherical wall when the narrow laser beam hits the spherical surface along its normal; light emitting diodes (LEDs) etc.

The sphere includes up to *N* equidistant radiation sources of this kind separated by a central angle of 360°/*N* – we shall consider the sphere with a single source, using the additivity principle and derive the radiation field produced by several sources through summation of the radiation fields produced by the each sources separately that have been rotated by appropriate angles. We also shall consider such source as point source with radiant intensity

$$I_s(\theta_s) = \frac{\nu+1}{2\pi}I_s(0)\cos^\nu\theta_s,$$

where $\theta_s$ is the angle between the direction of emission and the normal to the sphere surface, $\nu \in [0,\infty)$; $\nu = 1$ corresponds to a Lambertian point source. Due to the normalization factor $\dfrac{\nu+1}{2\pi}$, the source will have the same radiant flux for any value of $\nu$.


## 4. BRIEF DESCRIPTION OF THE MONTE CARLO ALGORITHM

### 4.1 Radiance calculation

The first application of our model and computational algorithm is the computation of sphere source radiance at a given point and in a given direction. For problems of this kind, algorithms employing forward ray tracing, where rays emitted by the source are traced until they escape the ISRS, are very inefficient. On the other hand, our assumption of an infinitesimal (point) source – makes backward ray tracing, where rays are originated at a point of observation and traced in opposite direction until they intercept the source, even more impractical. Hence we construct a new algorithm that employs backward ray tracing coupled with the "shadow rays" technique [16].

A key element of our algorithm is the analytical computation of irradiance produced by direct source radiation for each point of diffuse reflection. The irradiance at a point *P* of any surface is equal to

$$E(P) = \frac{V(P)I_s(\theta_S)\cos\theta_P}{d^2},$$

where *V(P)* is the vignetting function, which is equal to 1, if no obstruction exist between point *P* and the source, and to 0 – otherwise; $\theta_S$ and $\theta_P$ are angles between the normals to the ISRS surfaces at the point source and at the point *P*, respectively, and *d* is the distance between the point *P* and the source. The radiance of diffusely reflected radiation for irradiation of a surface computed by the previous equation, is equal to

$$L(P) = \frac{(\nu + 1)V(P)I_s(0)\cos^\nu \theta_S \cos\theta_P}{2\pi^2 d^2}$$

If 1, 2, 3, … is a series of intercepts obtained as a result of the application of the directional importance sampling method to the ISRS with all Lambertian surfaces, then

$$L_i(\theta) = L_{si}(\theta_{si})V_{si} + \rho_1\left(\frac{1}{\pi}E_{i1} + \rho_2\left(\frac{1}{\pi}E_{i2} + \rho_3\left(\frac{1}{\pi}E_{i3} + \rho_4\left(\frac{1}{\pi}E_{i4} + ...\right)\right)\right)\right)$$

$$= L_{is}(\theta_{is})V_{is} + \frac{1}{\pi}\left(\rho_1 E_{1i} + \rho_1\rho_2 E_{2i} + \rho_1\rho_2\rho_3 E_{3i} + \rho_1\rho_2\rho_3\rho_4 E_{4i} + ...\right)$$

$$= L_{is}(\theta_{is})V_{is} + \frac{1}{\pi}\sum_{j=1}^{m} E_{ij}\prod_{k=1}^{l_j}\rho_k$$

Averaging the realizations of $L_i(\theta)$ over a large number n of rays traced, we can write

$$L(\theta) = \frac{1}{n}\sum_{i=1}^{n}\left[L_s(\theta_{0i})V_{0i} + \frac{1}{\pi}\sum_{j=1}^{m_i} E_{ij}V_{ij}\prod_{k=1}^{l_{ij}}\rho^k\right],$$

where the first term in the brackets is the radiance of direct source radiation (if any), the second term is the sum of radiances produced by the source at the points of successive diffuse reflections by backward ray tracing. The flow chart for this algorithm is depicted in Figure 2.

We have computed the distribution of radiance over the ISRS aperture by tracing the rays from a point with coordinates $(0, 0, z_f)$ to the nodes of a rectangular grid superimposed on the plane of the exit port. All results shown in this paper correspond to such grid with coordinate *x* and *y*, normalized on the radius $R_a$ of exit port.

### 4.2 Irradiance calculation
We have also computed the distribution of irradiance in a plane normal to the ISRS axis at a coordinate location $z_p$, inside the circle of radius

$$R_p = \frac{R_a(z_p - z_f)}{z_f - z_a},$$

where

$$z_f = \frac{z_{b2}\left(z_a\sqrt{R^2 - z_{b1}^2} - R_a\right)}{z_{b2}\sqrt{R^2 - z_{b1}^2} - R_a}.$$

The irradiance inside this circle is determining by the radiation, incident from behind the target area of the ISRS. We superimpose a rectangular grid on this circle and compute the value of irradiance at each node with
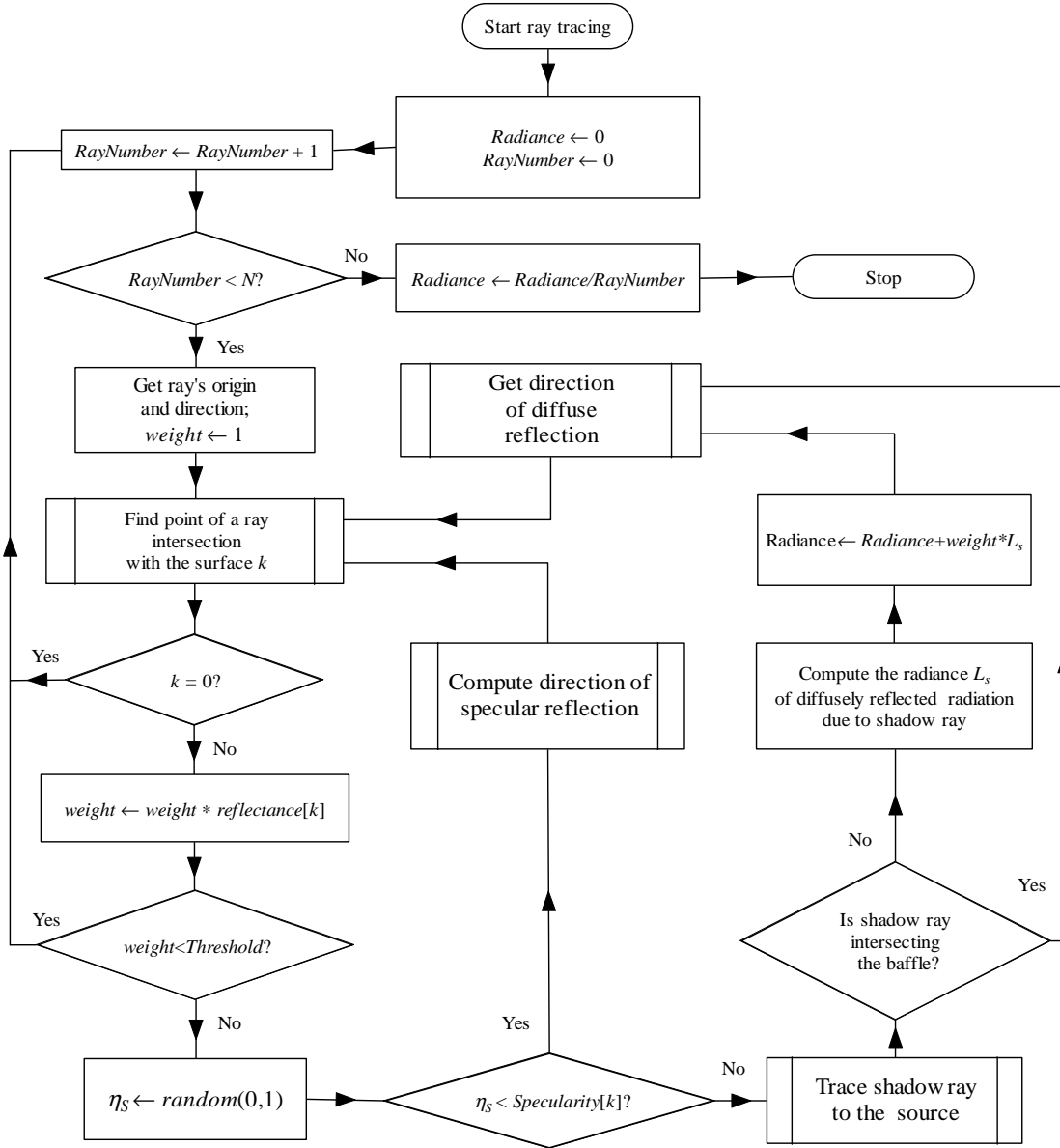
$$x^2 + y^2 < R_p^2.$$

Figure 2: Flow chart of "shadow rays" algorithm.

To do this, we generate points $(x_{ai}, y_{ai}, z_a)$ uniformly distributed over the sphere exit aperture and compute the radiance $L_{ik}$ at the node point $(x_{pi}, y_{pi}, z_p)$ in the direction, determined by the vector $\vec{\omega}_0$ with components

$$\begin{cases} \omega_{0x,ik} = (x_{ai} - x_{pk})/d_{ik}; \\ \omega_{0y,ik} = (y_{ai} - y_{pk})/d_{ik}; \\ \omega_{0z,ik} = (z_a - z_p)/d_{ik}, \end{cases}$$

where $d_{ik} = \sqrt{\left(x_{ai} - x_{pk}\right)^2 + \left(y_{ai} - y_{pk}\right)^2 + \left(z_a - z_p\right)^2}$ .

We compute the irradiance at every node using the equation

$$E\left(x_{pk}, y_{pk}, z_p\right) = \frac{\pi}{n} \sum_{i=1}^{n} L_{ik} \cos\theta_{ik} ,$$

where $n$ is the number of rays traced through the exit port from $k$-th node, $\theta_{ik}$ is the angle of incidence of $i$-th ray on $k$-th node.

# 5. DISCUSSION OF RESULTS

## 5.1 Input parameter data
The defining geometry parameter value are (all dimensions in mm): sphere radius $R = 202.3$; aperture radius $R_a = 37.5$; $z_a = 198.8$ (so that the flat diaphragm is absent); the coordinates of the conical baffle edges are $z_{b1} = -81.28$, $z_{b2} = -44.85$; $z_p = 350$. Using these data one can find $z_f = 288$, $R_p = 26.1$, and the full FOV from the point $(0, 0, z_f)$ is $45.6°$. We modeled the ISRS with modest values of wall reflectance – $0.9\ldots0.94$ that are appropriate for coatings designed for the infrared spectral range of 2 to 20 μm. Two main cases are examined: (i) the conical baffle and sphere are fabricated from the same diffuse material and (ii) baffle is fabricated from polished aluminum with reflectance $\rho = 0.985$ and specularity $S = 1$.

## 5.2 Evaluation of modeling accuracy
The convergence of results depends on several factors, such as the values of the geometrical parameters, the reflectance and specularity of the sphere's internal surfaces, as well as the number of rays traced and the maximum number of reflections of a ray. We have evaluated the computation accuracy of radiance and irradiance values using the standard technique of statistical processing of repeated measurements, treating the results of numerical experiments in the same manner as the results of measurements. In order to avoid any potential error due to ray trajectory truncation, we use a threshold value for statistical weight $\delta = 0.01\%$. For the purely diffuse sphere with $\rho_s = \rho_b = 0.9$, $10^5$ rays are enough to obtain a standard deviation of random uncertainty less than 0.1% in all cases examined in this paper. This corresponds to about 20 seconds per point running on a 2.2 GHz Pentium IV processor PC.

The above estimation is confirmed implicitly by the calculation of radiance distribution from Lambertian sphere with a Lambertian source and no baffle (such configuration has trivial analytical solution – uniform radiance distribution): for $\rho_s = 0.9$ we obtain the value of root-mean-square nonuniformity of about 0.05%.

## 5.3 Radiance distribution results
Some results of numerical experiments modeling radiance distributions are depicted in Color Plates A and B. In every column of color plates A and B the radiance distributions over the ISRS exit port produced by 1, 3, and 5 equidistant point sources are depicted. For the first rows, single radiation source is placed at the top of a picture.

We use rectangular grid with 51×51 nodes uniformly covering the exit port. The observation point is located at coordinates $(0, 0, z_f)$. We use the dimensionless coordinates $X = x/R_a$ and $Y = y/R_a$ and a bilinear interpolation [17] to obtain the color radiance map with the scale indicated at the side of each map. The program computes the normalized radiance $L'$ as the ratio of actual radiance $L$ to its mean value $\overline{L}$ for all $-1 < X, Y < 1$ and the standard deviations from the mean level $\overline{L'}$ by the equation

$$s = \sqrt{\frac{1}{m}\sum_{i=1}^{m}\left(L_i' - \overline{L'}\right)^2} \; ,$$

where $m$ is the number of nodes.

For purely diffuse sphere and Lambertian point source the best uniformity of irradiance distribution over internal spherical surface is attained by removing the baffle, thus there is no subject of optimization. Every deviation from cosine of the radiant intensity angular distribution for a point source placed on sphere's internal walls leads to uprising of nonuniformities, whose amplitude is maximal for the first reflection and decreases with reflection order growth. In this case, the use of internal baffle for prevention of direct irradiation of the sphere visible area by the source allows improving the uniformity of irradiance distribution over visible area.

The radiance distributions from purely diffuse ($S = 0$) ISRS and non-Lambertian point sources with $\nu = 2$ are presented in Color Plate A: the left columns corresponds to reflectance of all surfaces $\rho = 0.9$, the right one – to $\rho = 0.94$. The significant decrease of radiance nonuniformity (2 – 2.5 times) is achieved at the use of 3 symmetrically located radiation sources. The numerical experiments shown that the further increase of number of radiation sources doesn't lead to radiance distribution flattening. The explanation of this fact could be the following. All nonuniformities could be conditionally divided on radial and angular. Radial nonuniformities (like symmetrical inflations or valleys) in principle cannot be eliminated by the increase of number of sources.

In the left column of Color Plate B, the radiance distributions from diffuse sphere with $\rho = 0.9$ and specular ($S = 1$) baffle with $\rho = 0.985$ are depicted. The results of modeling show that the use of specular baffle improves the radiance distribution nonuniformity as compared with the purely diffuse ISRS.

The case of all diffuse surfaces with $\rho = 0.9$ and non-Lambertian point sources with $\nu = 3$ is depicted in the right column of Color Plate B. Such source with $\cos^2\theta$ dependence of radiant intensity on incidence angle produces radial rather than angular nonuniformities. Note that artifactual patterns on the several maps for 3 and 5 sources are due to the moiré effect for discrete images.

The numerical experiments performed for non-zero specularities of sphere's walls (these results are not included into Color Plates) shown the existence of high and acute peak at the center of exit port. This peak is unobservable in experiments and is an effect of too rough approximation of real BRDF of materials in the infrared region by the specular-diffuse model.

## 5.4 Irradiance distribution results

In every column of color plate C the irradiance distributions over the circle of radius $R_p$ in the plane $z = z_p$ produced by 1, 3, and 5 equidistant point sources are depicted. As in the case of radiance modeling of distributions, we use a bilinear interpolation between $51 \times 51$ nodes of rectangular grid and the dimensionless coordinates $X = x/R_p$ and $Y = y/R_p$. The program calculates the normalized irradiance $E'$ as the ratio of actual irradiance $E$ to its mean value $\overline{E}$ for all $-1 < X, Y < 1$, as well as the standard deviations from the mean level $\overline{E'}$ by the equation

$$s = \sqrt{\frac{1}{m}\sum_{i=1}^{m}\left(E_i' - \overline{E'}\right)^2} \; .$$

In the left column of Color Plate C, the irradiance distributions from ISRS with all diffuse surfaces and ρ = 0.9 are depicted. Due to high angular uniformity (axial symmetry), an increase in the number of radiation sources can't appreciably change the value of $s \approx 0.97\%$.

The case of a specular baffle having ρ = 0.985 shows an initially (for a single radiation source) small irradiance nonuniformity of about 0.4%. The joint action of 3 symmetrically placed sources decreases this value down to 0.17%.

## 6.  CONCLUSIONS

We have described an approach to computer modeling of the ISRS with several point radiation sources. A Monte Carlo algorithm and appropriate software for the computation of radiance and irradiance distributions produced by the ISRS have been developed. Preliminary parametric studies of the influence of important factors such as the reflectance and specularity of the sphere and baffle, the number of point sources and the angular distribution of radiant intensity, have been performed.

The analysis of results obtained enables us to select the directions of further research and computational model improvement. We plan to change the model of the source from a single point to a more realistic extended source one. The numerical experiments performed with the specular-diffuse model of sphere wall reflectance show the necessity of improvement to the use of real BRDF as input data to modeling.
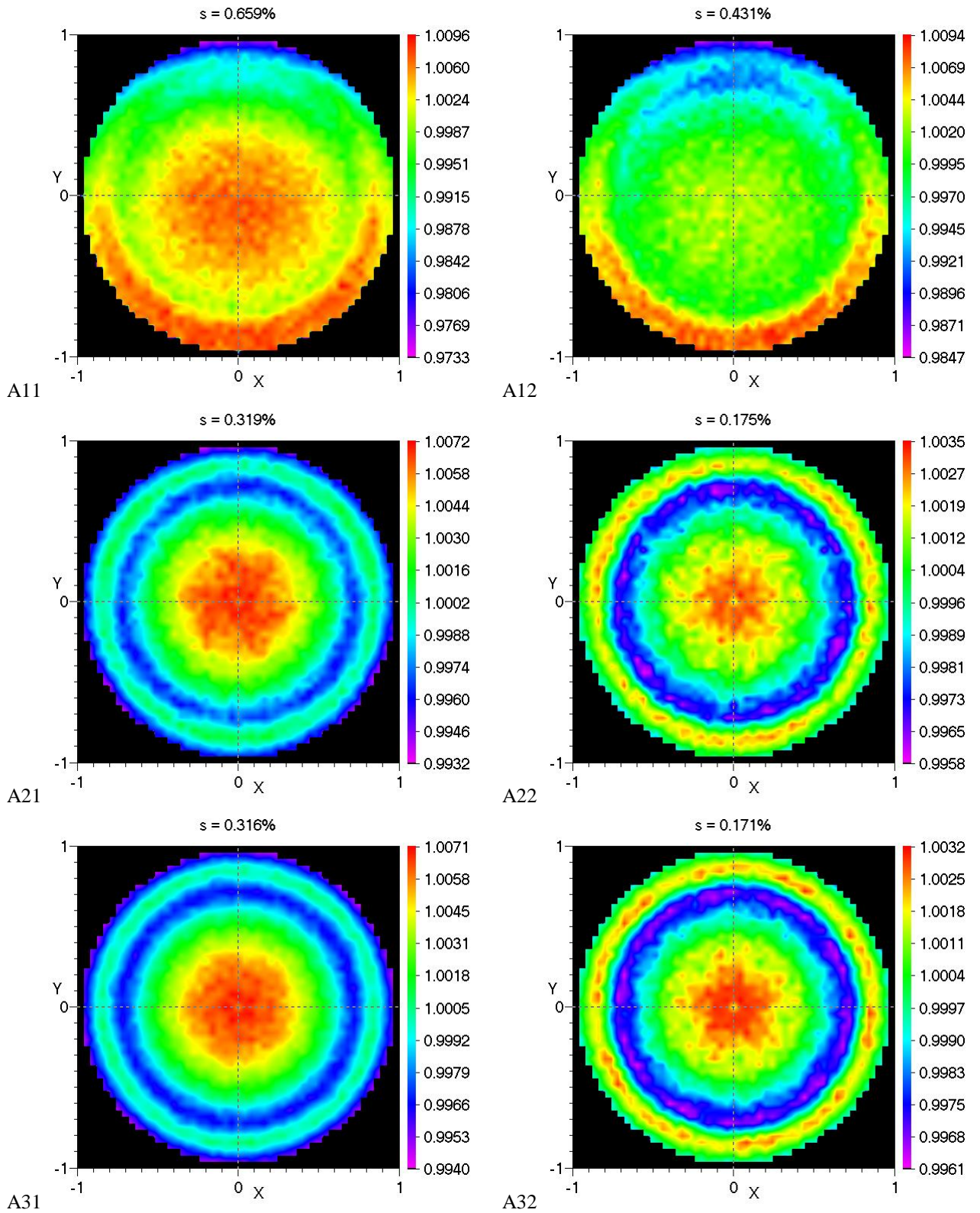
## REFERENCES

1. S. W. Brown, G. P. Eppeldauer, K. R. Lykke, "NIST facility for Spectral Irradiance and Radiance Responsivity Calibrations with Uniform Sources", *Metrologia*, **37**, pp. 579-582, 2000
2. K. R. Lykke, P.-S. Show, L.M. Hanssen, G. P. Eppeldauer, "Development of a monochromatic, uniform source facility for calibration of radiance and irradiance detectors from 0.2 μm to 12 μm", *Metrologia*, **35**, pp. 479-484, 1998
3. J. E. Clare, "Comparison of four analytic methods for the calculation of irradiance in integrating spheres", *J. Opt. Soc Am. A*, **15**, No. 12, pp. 3086-3096, 1998
4. J. E. Clare, "Analytic calculation of irradiance in integrating spheres with a flat port", *CIE 24th Sessions*, *Warsaw '99*, pages 166-170, 1999
5. H. L. Tardy, "Matrix method for integrating-sphere calculations", *J. Opt. Soc Am. A*, **8**, No. 9, 1411-1418, 1991
6. D. G. Goebel, "Generalized Integrating-Sphere Theory", *Applied Optics*, **6**, No. 1, pp. 125-128, 1967
7. L. M. Hanssen, "Effects of non-Lambertian surfaces on integrating sphere measurements", *Applied Optics*, **35**, No. 19, pp. 3597-3606, 1996
8. B. G. Crowther, "Computer modeling of integrating spheres", *Applied Optics*, **35**, No. 30, pp. 5880-5886, 1996
9. B. G. Crowther, K. J. Thome, S. F. Biggar, C. J. Burkhart, "Internally-baffled integrating sphere cosine collector", *Proc. SPIE*, **3117**, pp. 246-252, 1997
10. A. V. Prokhorov, V. I. Sapritsky, S. N. Mekhontsev, "Modeling of integrating spheres for photometric and radiometric applications", *Proc. SPIE*, **2815**, pp. 118-125, 1996
11. V. Pohl, V. Jungnickel, R. Hentges, C. von Helmolt, "Integrating Sphere Diffuser for Wireless Infrared Communication", *Proc. IEE Colloquim Optical Wireless Communications*, pp.4/1-4/6, London, June 22, 1999
12. A. Ziegler, H. Hess, H. Schimpl, "Rechnersimulatiom von Ulbrickugeln", Optik, **101**, No. 3, pp. 130-136, 1996 (in German)
13. A. Prokhorov, S. Mekhontsev, L. Hanssen, "Evaluation of performance of integrating sphere for indirect emittance measurement", *Proc. TEMPMEKO 2001, 8th International Symposium on Temperature and Thermal Measurements in Industry and Science*, Vol. 1, pp. 277-282, 19-21 June 2001, Berlin, Germany
14. R. Siegel, J. R. Howell, *Thermal Radiation Heat Transfer*, 3rd Ed., Taylor & Francis, Washington, DC, 1992
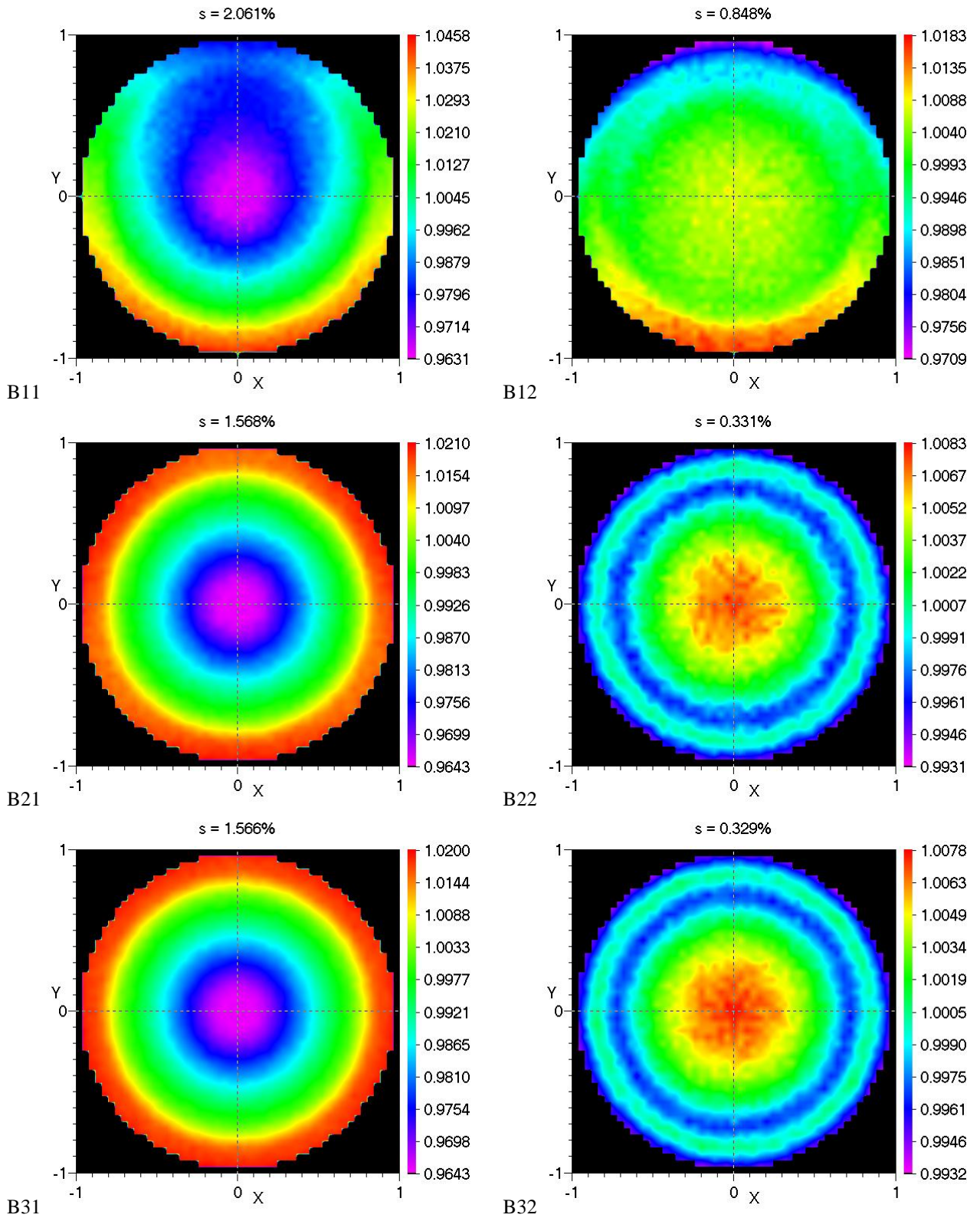
15. G. Marsaglia, "Choosing a point from the surface of a sphere", *The Annals of Mathematical Statistics*, **43**, No. 2, pp. 645-646, 1972

16. P. Shirley, *Realistic Ray Tracing*, A K Peters, Natick, MA, 2000, 165 pp.

17. W. H. Press, S. A. Teukolsky, W. T. Vetterling, B. P. Flannery, *Numerical Recipes in C++. The Art of Scientific Computing*. 2nd Ed., Cambridge University Press, 2002

* hanssen@nist.gov; phone 1 301 975 2344; fax 1 301 840 8551; http://www.nist.gov; NIST, Bldg 220 Room A-305, 100 Bureau Dr., Stop 8442, Gaithersburg, MD 20899-8442

**Color Plate A.**

s = 0.659%

s = 0.431%

A11

A12

s = 0.319%

s = 0.175%

A21

A22

s = 0.316%

s = 0.171%

A31

A32

# Color Plate B.

s = 2.061%

B11

s = 0.848%

B12

s = 1.568%

B21

s = 0.331%

B22

s = 1.566%

B31

s = 0.329%

B32

**Color Plate C.**



C11

C12

C21

C22

C31

C32